RSC Advances

PAPER

View Article Online
View Journal | View Issue

Cite this: *RSC Adv.*, 2024, **14**, 3186

A simple and reliable QSPR model for prediction of chromatography retention indices of volatile organic compounds in peppers†

Shahin Ahmadi, *[a] Shahram Lotfi, [b] Hamideh Hamzehali[c] and Parvin Kumar [d]

Worldwide, various types of pepper are used in food as an additive due to their unique pungency, aroma, taste, and color. This spice is valued for its pungency contributed by the alkaloid piperine and aroma attributed to volatile essential oils. The essential oils are composed of volatile organic compounds (VOCs) in different concentrations and ratios. In chromatography, the identification of compounds is done by comparing obtained peaks with a reference standard. However, there are cases where reference standards are either unavailable or the chemical information of VOCs is not documented in reference libraries. To overcome these limitations, theoretical methodologies are applied to estimate the retention indices (RIs) of new VOCs. The aim of the present work is to develop a reliable QSPR model for the RIs of 273 identified VOCs of different types of pepper. Experimental retention indices were measured using comprehensive two-dimensional gas chromatography coupled to quadrupole mass spectrometry (GC × GC/qMS) using a coupled BPX5 and BP20 column system. The inbuilt Monte Carlo algorithm of CORAL software is used to generate QSPR models using the hybrid optimal descriptor extracted from a combination of SMILES and HFG (hydrogen-filled graph). The whole dataset of 273 VOCs is used to make ten splits, each of which is further divided into four sets: active training, passive training, calibration, and validation. The balance of correlation method with four target functions *i.e.* TF0 (WIIC = WCII = 0), TF1 (WIIC = 0.5 & WCII = 0), TF2 (WIIC = 0 & WCII = 0.3) and TF3 (WIIC = 0.5 & WCII = 0.3) is used. The results of the statistical parameters of each target function are compared with each other. The simultaneous application of the index of ideality of correlation (IIC) and correlation intensity index (CII) improves the predictive potential of the model. The best model is judged on the basis of the numerical value of R^2 of the validation set. The statistical result of the best model for the validation set of split 6 computed with TF3 (WIIC = 0.5 & WCII = 0.3) is R^2 = 0.9308, CCC = 0.9588, IIC = 0.7704, CII = 0.9549, Q^2 = 0.9281 and RMSE = 0.544. The promoters of increase/decrease for RI are also extracted using the best model (split 6). Moreover, the proposed model was used for an external validation set.

Received 21st November 2023
Accepted 3rd January 2024

DOI: 10.1039/d3ra07960k

rsc.li/rsc-advances

1. Introduction

Peppers are among the most ancient spices known to man and are extensively harvested all over the entire globe. Pepper fruits contain a high quantity of constituents advantageous to human health, such as antioxidants, minerals, vitamins (mainly A, C, and E), polyphenols and carotene. All types of pepper are eaten fresh or dried and are used in the food industry as additives (coloring and flavoring agents) because of their unique pungency, color, flavor, and aroma.[1–3] The piperine alkaloid (as the (*E*,*E*)-isomer), which is responsible for pungency, and the volatile essential oils that provide flavour and aroma are primarily accountable for the quality of peppers as rated by humans.[4,5] However, other compounds have also been identified in peppers, such as terpenes, flavonoids, steroids, unsaturated fatty acids, and polysaccharides. Furthermore, the essential oil derived from the distillation of pepper contains various taste and flavouring components: *e.g.* oxygenated monoterpenoid compounds, monoterpene hydrocarbons and oxygenated compounds, sesquiterpene hydrocarbons and oxygenated compounds, oxygenated sesquiterpenes, and phenolic compounds. These compounds are designated as volatile organic compounds (VOCs).[4,6,7] The essential oils of peppers can also be employed as antioxidant, antiseptic, antibacterial, antimycotic, anti-epileptic, anti-inflammatory, diuretic, antipyretic, anthelminthic, and carminative agents.[8,9]

[a]*Department of Pharmaceutical Chemistry, Tehran Medical Sciences, Islamic Azad University, Tehran, Iran. E-mail: ahmadi.chemometrics@gmail.com*
[b]*Department of Chemistry, Payame Noor University (PNU), 19395-4697 Tehran, Iran*
[c]*Department of Chemistry, Islamic Azad University, East Tehran Branch, Tehran, Iran*
[d]*Department of Chemistry, Kurukshetra University, Kurukshetra, Haryana, 136119, India*

† Electronic supplementary information (ESI) available. See DOI: https://doi.org/10.1039/d3ra07960k

Numerous reports have been published for the identification and characterization of diverse VOCs of peppers.[10–13] Gas chromatography (GC) and gas chromatography-mass spectrometry (GC-MS) techniques are generally employed for the quantitative determination of volatile compounds in peppers.[14,15] Other techniques such as proton-transfer-reaction time-of-flight mass spectrometry (PTR-ToF-MS), two-dimensional gas chromatography with flame ionization detection (GC × GC-FID), quadrupole mass spectrometry (GC × GC-qMS) and time-of-flight mass spectrometry (GC × GC/TOFMS) are also applied to identify VOCs.[5,10,16]

In chromatography, the chemical structure of compounds is identified by comparing obtained peaks with a reference standard. However, in some cases, reference standards may be unavailable or the chemical information about VOCs may not be registered in reference libraries. To reduce these limitations, theoretical techniques for estimating the retention index (RI) of new VOCs are employed. Hence, the quantitative structure–property/activity relationship (QSPR/QSAR) is employed to predict the retention index (RI).[17] QSPR/QSAR is a significant theoretical technique used to establish mathematical models that predict the properties/activities or endpoints of compounds, which have been newly designed or are undeveloped.[18,19]

A literature survey revealed that CORAL (CORrelation And Logic software available at **http://www.insilico.eu/coral**) software can be implemented for the development of predictive QSPR/QSAR models. CORAL is freeware software designed to calculate one-variable QSPR/QSAR models between an endpoint and descriptors using the Monte Carlo algorithm. In this software, the optimal descriptor of correlation weight (DCW) is calculated using the SMILES (Simplified Molecular-Input Line-Entry System) notation of the molecular structure.[20–22] According to a literature report, the index of ideality of correlation (IIC) and correlation intensity index (CII) are applied as new criteria for judging the predictive potential of the QSPR model. It is often mentioned in the literature that the numerical value of the coefficient of determination (R^2) for the validation and calibration set is improved by the IIC, whereas the CII improves the numerical value of the coefficient of determination (R^2) for all four sets: *i.e.* active training, passive training, calibration and validation.[23–31]

The objective of this study is to construct a predictive QSPR model using the Monte Carlo technique of the CORAL software for the retention index property of 273 VOCs recognized in peppers. Ten random splits are made and each split is divided into four subsets. The IIC and CII statistical parameters are employed to predict a better model. The balance of correlation method with four target functions, *i.e.* TF0 ($W_{IIC} = W_{CII} = 0$), TF1 ($W_{IIC} = 0.5$ & $W_{CII} = 0$), TF2 ($W_{IIC} = 0$ & $W_{CII} = 0.3$) and TF3 ($W_{IIC} = 0.5$ & $W_{CII} = 0.3$), is used to examine the robustness and accuracy of the constructed QSPR model.

2. Data and method

2.1. Data

The retention index (RI) data for 273 VOCs identified in 13 peppers were obtained from the literature by Rojas *et al.*[32] Polydimethylsiloxane/divinylbenzene (PDMS/DVB) fiber was used for extraction of the VOCs. The peaks on the two-dimensional GC with a quadrupole mass spectrometric detection (GC × GC-qMS) chromatogram were identified by the column set comprising a non-polar molecule (5% phenyl polysilphenylenesiloxane) as the primary column and a polar molecule (polyethylene glycol) in the second column. Experimental retention indices were obtained using the van den Dool and Kratz equation and Adams' retention indices. Data preprocessing details were reported in the literature by Rojas *et al.*[32] The range of values for the retention index (RI) went from 930 to 1790. The IDs of the compound, SMILES codes, and corresponding experimental and predicted RI are provided in Table S1.† Ten splits were prepared and each split was further split randomly into four subsets: *i.e.* an active training set (≈26%), a passive training set (≈20%), a calibration set (≈20%), and a validation set (≈34%). The role of each set was fixed and is well explained in the literature.[33–36]

2.2. Method

The methodology for obtaining the results from the CORAL software can be summarized as a group by the following steps:

(1) Data preparation involves converting the structure to SMILES and preparing the Total set file.

(2) The process of data splitting in CORAL software is carried out using random splitting. This can be done using the classical scheme or balance of correlation. In the balance of correlation the data is divided into four sets: active training, passive training, calibration, and validation sets. However, if the amount of data is small, the classical scheme is used and the data set includes training, calibration, and validation sets.

(3) The selection of descriptors is based on either SMILES or a graph, or a combination of both. The descriptors are chosen accordingly.

(4) The target function selection involves computing correlation weights using the Monte Carlo method and maximizing one of the target functions: namely TF0, TF1, TF2, or TF3. The formulas of these target functions are described in the corresponding section.

(5) Model building consists of two phases. In Phase 1, the preferable threshold and number of epochs are searched for using Monte Carlo optimization based on statistical results from the calibration set. In Phase II, the preferable model is constructed after optimization of the threshold and number of epochs.

(6) External validation is performed on the test sets after model building.

(7) Model interpretation is carried out in this step.

(8) New molecules can be designed based on the model interpretation.

2.3. Hybrid optimal descriptor

As previously mentioned in the preceding section, in CORAL software three types of optimal descriptors can be calculated: *i.e.*, SMILES-based, graph-based, and hybrid descriptors

(obtained by combining SMILES and graph-based). The graph-based descriptor can be computed by using a hydrogen-filled graph (HFG), a hydrogen-suppressed molecular graph (HSG) or a graph of atomic orbitals (GAO).[37–39] A literature survey shows that QSPR models designed using the hybrid optimal descriptor provide robust models with higher statistical quality.[40] Here, the QSPR model for the prediction of RI is designed by utilizing a hybrid optimal descriptor based on the correlation weights of SMILES attributes and vertex degrees in the hydrogen-filled graph (HFG).

The hybrid optimal descriptor of the correlation weights (DCW) is computed using the following equation:

$$\mathrm{DHybridCW(T^*,N^*)} = \mathrm{DCW_{SMILES}(T^*,N^*)} + \mathrm{DCW_{HFG}(T^*,N^*)} \quad (1)$$

The DCW of HFG and SMILES are calculated *via* mathematical eqn (2) and (3).

$$\mathrm{DCW_{SMILES}(T^*,N^*)} = \sum \mathrm{CW}(S_k) + \sum \mathrm{CW}(\mathrm{SS_k}) + \sum \mathrm{CW}(\mathrm{SSS_k}) + \mathrm{CW(BOND)} + \mathrm{CW(MFCs)} \quad (2)$$

$$\mathrm{DCW_{HFG}(T^*,N^*)} = \sum \mathrm{CW}(\mathrm{EC0_k}) + \sum \mathrm{CW}(\mathrm{EC1_k}) + \sum \mathrm{CW}(\mathrm{pt2_k}) + \sum \mathrm{CW}(\mathrm{VS2_k}) + \sum \mathrm{CW}(\mathrm{nn_k}) + \sum \mathrm{CW(C5)} + \sum \mathrm{(C6)} \quad (3)$$

In eqn (2), the structural attributes S_k, $\mathrm{SS_k}$, and $\mathrm{SSS_k}$ are single SMILES symbols (*e.g.*, Cl or S), two SMILES symbols and a combination of three SMILES symbols, respectively. The BOND code demonstrates the existence or absence of double (=), triple (#), or stereochemical bonds (@ or @@). Here, the molecular feature contributions (MFCs) are the total number of oxygen atoms (O), the number of double bonds (=), and the number of triple bonds (#). Therefore, in eqn (3), the attributes EC0 and EC1 are the number of neighbors of a vertex degree and Morgan's connectivity of first order; $\mathrm{pt2_k}$ is the number of paths of length 2; VS2 is the valence shells of radius 2 in the HFG; the nn symbol implies nearest neighbors; C5 and C6 are descriptors that represent the five- and six-membered rings in the molecular structure, respectively. T is the threshold to separate SMILES attributes into noise or active. The active SMILES are applied to construct the model. The noise SMILES are not involved in constructing the model. T^* and N^* are the optimum threshold and number of epochs of the Monte Carlo optimization method. T^* and N^* provide the maximum statistical quality for the calibration set. The numerical values for CWs are acquired from the Monte Carlo optimization and the optimal descriptor is computed with the optimal CWs. Then the calculated CWs are employed to design a predictive model of the RI according to the following equation:

$$\mathrm{RI} = \mathrm{C_0} + \mathrm{C_1} \times \mathrm{DCW(T^*,N^*)} \quad (4)$$

2.4. The Monte Carlo optimization

Here to design robust QSPR models, four different kinds of target functions, TF0, TF1, TF2 and TF3, are used. Then, the outcomes of the statistical results are compared with each other.

The mathematical equations for each target function can be demonstrated follows:

$$\mathrm{TF_0} = \mathrm{R_{ATRN}} + \mathrm{R_{PTRN}} - |\mathrm{R_{ATRN}} - \mathrm{R_{PTRN}}| \times \mathrm{dr_{weight}} \quad (5)$$

$$\mathrm{TF_1} = \mathrm{TF_0} + \mathrm{IIC_{CAL}} \times \text{weight for IIC } (\mathrm{IIC_{weight}}) \quad (6)$$

$$\mathrm{TF_2} = \mathrm{TF_0} + \mathrm{CII_{CAL}} \times \text{weight for CII } (\mathrm{CII_{weight}}) \quad (7)$$

$$\mathrm{TF_3} = \mathrm{TF_0} + \mathrm{IIC_{CAL}} \times \mathrm{IIC_{weight}} + \mathrm{CII_{CAL}} \times \mathrm{CII_{weight}} \quad (8)$$

Here, R_{ATRN} and R_{PTRN} are the correlation coefficients between the observed and predicted RI for the active training and passive training sets, respectively. The numerical values for weights of index of ideality of correlation (IIC) and correlation intensity index (CII) are usually kept constant and here the numerical values of $\mathrm{dr_{weight}}$, $\mathrm{IIC_{weight}}$ and $\mathrm{CII_{weight}}$ were 0.1, 0.5 and 0.3, respectively. $\mathrm{IIC_{CAL}}$ and $\mathrm{CII_{CAL}}$ are computed for the calibration set using eqn (9).

$$\mathrm{IIC_{CAL}} = R_{\mathrm{CAL}} \times \frac{\min\left({}^{-}\mathrm{MAE_{CAL}}, {}^{+}\mathrm{MAE_{CAL}}\right)}{\max\left({}^{-}\mathrm{MAE_{CAL}}, {}^{+}\mathrm{MAE_{CAL}}\right)} \quad (9)$$

R_{CAL} is the correlation coefficient between experimental values and calculated values of RI for the calibration set. The negative and positive mean absolute errors are indicated by ${}^{-}$MAE and ${}^{+}$MAE, which are computed as follows:

$${}^{-}\mathrm{MAE_{CAL}} = -\frac{1}{N}\sum_{y=1}^{N^-} |\Delta_k| \quad \Delta_k < 0,\ {}^{-}N \text{ is the number of } \Delta_k < 0 \quad (10)$$

$${}^{+}\mathrm{MAE_{CAL}} = +\frac{1}{N}\sum_{y=1}^{N^+} |\Delta_k| \quad \Delta_k \geq 0,\ {}^{+}N \text{ is the number of } \Delta_k \geq 0 \quad (11)$$

$$\Delta_k = \mathrm{observed_k} - \mathrm{calculated_k} \quad (12)$$

The 'k' is the index (1, 2, …, N) and the $\mathrm{observed_k}$ and $\mathrm{calculated_k}$ are related to the endpoint.

$$\mathrm{CII_{CAL}} = 1 - \sum \mathrm{Protest_K}$$

$$\mathrm{Protest_K} = \begin{cases} R_k{}^2 - \mathrm{R}^2, & \text{if } R_k{}^2 - R^2 > 0 \\ 0 & \text{otherwise} \end{cases} \quad (13)$$

R^2 is the correlation coefficient for a set that contains n substances. $R_k{}^2$ is the correlation coefficient for $n - 1$ substances of a set after removing the kth substance. Hence, if $(R_k{}^2 - R^2)$ is greater than zero, the kth substance is an "oppositionist" for the correlation between experimental and predicted values of the set. A small sum of "protests" means a more "intensive" correlation.

2.5. Applicability domain

In QSPR/QSAR models, the applicability domain (AD) is used to specify whether the designed model interpolates (correct predictions) or extrapolates (incorrect predictions). In the CORAL software, the distribution of SMILES attributes in the active training, passive training, and calibration sets is used to calculate the AD. Therefore, the AD for the model acquired as a result of Monte Carlo optimization varies depending on the distribution of the datasets in the training and calibration sets. In the QSPR/QSAR models designed by CORAL software, the statistical defects of SMILES are employed to define the AD. The "statistical defect," d(A) is computed according to the following mathematical equation:

$$\text{Defect}_{A_K} = \begin{cases} \dfrac{|P_{ATRN}(A_K) - P_{PTRN}(A_K)|}{N_{ATRN}(A_K) + N_{PTRN}(A_K)} + \dfrac{|P_{ATRN}(A_K) - P_{CAL}(A_K)|}{N_{ATRN}(A_K) + N_{CAL}(A_K)} + \dfrac{|P_{PTRN}(A_K) - P_{CAL}(A_K)|}{N_{PTRN}(A_K) + N_{CAL}(A_K)} & \text{If } A_K = 0 \\ \text{Defect}_{A_K} & \text{If } A_K = 0 \end{cases} \quad (14)$$

$P_{ATRN(Ak)}$, $P_{PTRN(Ak)}$ and $P_{CAL(Ak)}$ are the probability of attributes in the active training set, passive training set, and calibration set, respectively; $N_{ATRN(Ak)}$, $N_{PTRN(Ak)}$, and $N_{CAL(Ak)}$ are frequencies of attributes in the active training, passive training and calibration sets, respectively.

The SMILES-statistical defect (D) can be calculated as the sum of statistical defects of all attributes:

$$\text{Defect}_{\text{Molecule}} = \sum_{k=1}^{NA} \text{Defect}_{A_K} \quad (15)$$

NA is the number of active SMILES attributes for the given compounds.

In CORAL, a SMILES is an outlier if:

$$\text{Defect}_{\text{molecule}} > 2 \times \overline{\text{Defect}}_{\text{ATRN}} \quad (16)$$

$\overline{\text{Defect}}_{\text{ATRN}}$ D is an average of statistical defects for the dataset of the active training set.

3. Results and discussion

3.1. QSPR modelling for RI

Based on ten initial QSPR models, three compounds (compounds 49, 205, and 265) were identified as outliers. Therefore, these compounds were excluded from the data set before further processing. Herein, to achieve consistent statistical performance, ten different QSPR models were built for each type of target function (TF_0, TF_1, TF_2, and TF_3) employing hybrid optimal descriptors. The summary of statistical results for all QSPR models is summarized in Table S2.† The numerical value of R^2 calculated with TF_3 for the validation set of all splits is higher than the R^2 calculated with the other target functions (TF_0, TF_1 and TF_2); thus the TF_3 calculated with eqn (8) was selected as the best target function. A comparison of the determination coefficients of the validation set for all splits computed *via* four target functions is represented in Fig. 1.

The QSPR models for the ten splits formulated with TF_3 for prediction of the RI of the VOCs are given below:

Split 1

$$RI = 73.8025(\pm 7.0844) + 24.5924(\pm 0.1499) \times DCW(1,15) \quad (17)$$

Split 2

$$RI = 121.5622(\pm 6.8196) + 26.4093(\pm 0.1507) \times DCW(1,15) \quad (18)$$

Split 3

$$RI = 315.0484(\pm 6.5146) + 20.0374(\pm 0.1270) \times DCW(1,15) \quad (19)$$

Split 4

$$RI = 133.8434(\pm 9.0780) + 16.6644(\pm 0.1272) \times DCW(1,15) \quad (20)$$

Split 5

$$RI = 120.8001(\pm 5.6911) + 22.7349(\pm 0.1122) \times DCW(1,15) \quad (21)$$

Split 6

$$RI = 265.7739(\pm 6.3219) + 23.9520(\pm 0.1477) \times DCW(1,15) \quad (22)$$

Split 7

$$RI = 107.8894(\pm 7.4311) + 23.2382(\pm 0.1417) \times DCW(1,15) \quad (23)$$

Split 8

$$RI = 40.7742(\pm 6.0698) + 25.9964(\pm 0.1255) \times DCW(1,20) \quad (24)$$

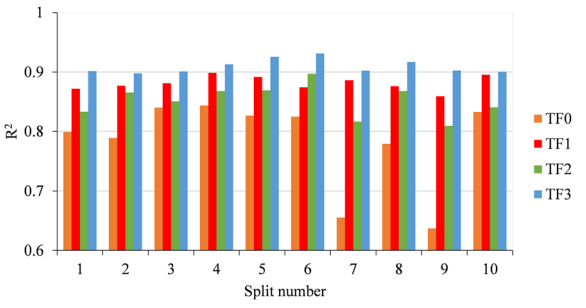

Fig. 1 Comparison of determination coefficients computed with TF0, TF1, TF2 and TF3 of all ten splits.

Split 9

$$RI = 25.2594(\pm 6.5441) + 25.5860(\pm 0.1587) \times DCW(1,15) \quad (25)$$

Split 10

$$RI = 110.5639(\pm 6.0444) + 21.8635(\pm 0.1077) \times DCW(1,15) \quad (26)$$

3.2. Model validation

In this study, the RI of the VOCs was predicted using QSPR models based on Monte Carlo optimization employing four target functions TF_0 ($W_{IIC} = W_{CII} = 0$), TF_1 ($W_{IIC} = 0.5$ & $W_{CII} = 0$), TF_2 ($W_{IIC} = 0$ & $W_{CII} = 0.3$) and TF_3 ($W_{IIC} = 0.5$ &$W_{CII} = 0.3$), and each target function was checked with ten random splits. The balance of correlation method was applied to generate QSPR models. The statistical results presented in Table S2† indicate that all designed QSPR models are within the standard range in terms of statistical criteria and have robust predictability. It can also be seen from Table S2† that simultaneously adding the weight IIC and CII to the target function increases its ability to predict RI as well as improving the statistical results. The numerical value of R^2 for the validation set of split 6 ($R^2 = 0.9308$, eqn (22)) was found to be higher than the numerical value of R^2 for the other models created with TF3, so it was identified as the best model. Fig. 2 displays the plot between observed and calculated data of the RI for the QSPR models computed with TF_3. A good correlation between observed RI and calculated RI, as well as a uniform distribution of RI for active training, passive training, calibration and validation sets can be seen in Fig. 2. Finally, the validation metrics for each model are calculated using three strategies: (i) internal validation or cross-validation with the training set data; (ii) external validation with the test set data; and (iii) Y-scrambling or data randomization. If $CR^2p > 0.5$ for the created model in a Y-randomization test, the model is free of chance correlation. For all constructed QSPR models the numerical value of CR^2p was more than 0.5, indicating the robustness of the developed models.

3.3. Interpretation of the QSPR model

In the QSPR model developed by the CORAL software, mechanistic interpretation is defined as the description of structural attributes acquired from SMILES or hydrogen-filled graphs which are responsible for the increase or decrease of an endpoint. If the numerical value of correlation weights of these structural attributes is negative in three or more runs of the optimization, then these structural features are defined as a promoter of endpoint decrease. On the other hand, if the numerical value of correlation weights of these structural attributes is positive in three or more runs of the optimization, then these structural features are defined as a promoter of endpoint increase. However the structural attribute is undefined if the correlation weight of the structural descriptors has both positive and negative numerical values.

The promoters for endpoint RI increase or decrease were computed from the best model (split 6) and are displayed in Table 1. Morgan extended connectivity of zero-order for hydrogen atom as 1 (ec0-h…1…), Morgan extended connectivity of first-order for hydrogen atom as 4 (ec1-h…4…), Morgan extended connectivity of first-order for carbon atom as 7 (ec1-c…7…), Morgan extended connectivity of zero-order for carbon atom as 3 (ec0-c…3…), Morgan extended connectivity of first-order for carbon atom as 4 (ec1-c…10…), the number of paths of length 2 which started from a hydrogen atom is equal to 3 (pt2-h…3…), the number of paths of length 2 which started from a carbon atom is equal to 5 (pt2-c…5…), the number of paths of length 2 which started from a hydrogen atom is equal to 2 (pt2-h…2…), two sp3 hybridized carbon joined by branching (c…(…c…), the presence of two consecutive aliphatic carbons (c…c…) *etc.* were some significant promoters of endpoint increase. The nearest neighbours code for carbon equal to 413 (nnc-c…413), the nearest neighbours code for carbon equal to 440 (nnc-c…440), a combination of the carbon atom, oxygen and branching (c…o…(…), and 28 as a sum of vertex degrees which take place at a topological distance of 2 relatively to carbon vertex (*vs.* 2-c…28) *etc.* were some significant promoters of endpoint decrease.

3.4. A comparison of various QSPR models based on RI

A survey of the literature indicates that Rojas *et al.* (2019) reported only one QSPR model for retention index: the QSPR model for 273 VOCs of pepper.[32] The molecular descriptors and molecular fingerprints were calculated using Dragon and PaDEL-Descriptor software. To create balanced subsets, the dataset was divided into training, validation, and test sets of molecules using the Balanced Subsets Method (BSM). Afterward, the Wootton, Sergent, and Phan-Tan-Luu (WSP) unsupervised variable reduction method was employed to reduce the presence of multicollinearity, redundancy, and noise among the initial pool of 4336 molecular descriptors and fingerprints. By implementing this method, a reduced pool consisting of 1664 descriptors was subjected to supervised selection through replacement method (RM) variable subset selection in order to establish a four-descriptor model. The efficacy of the model was assessed by evaluating the coefficient of determination and the root-mean-square deviation in fitting. Specifically, the values obtained for R^2 and RMSD for training were 0.879 and 72.1, respectively. Similarly, R^2 and RMSD were found to be 0.832 and 91.7 in the validation set, while R^2 and RMSD were 0.915 and 55.4 in the test set. The minimal discrepancies observed among these parameters across the three sets indicate the stability and predictability of the QSPR model.

Table 2 displays a comparison of the statistical results of the present QSPR model with the reported QSPR model. The previously reported model was implemented with only one split, but in the present QSPR models, 10 splits were used to design 40 QSRR models employing four target functions (TF0, TF1, TF2 and TF3). Two significant criteria, the index of ideality

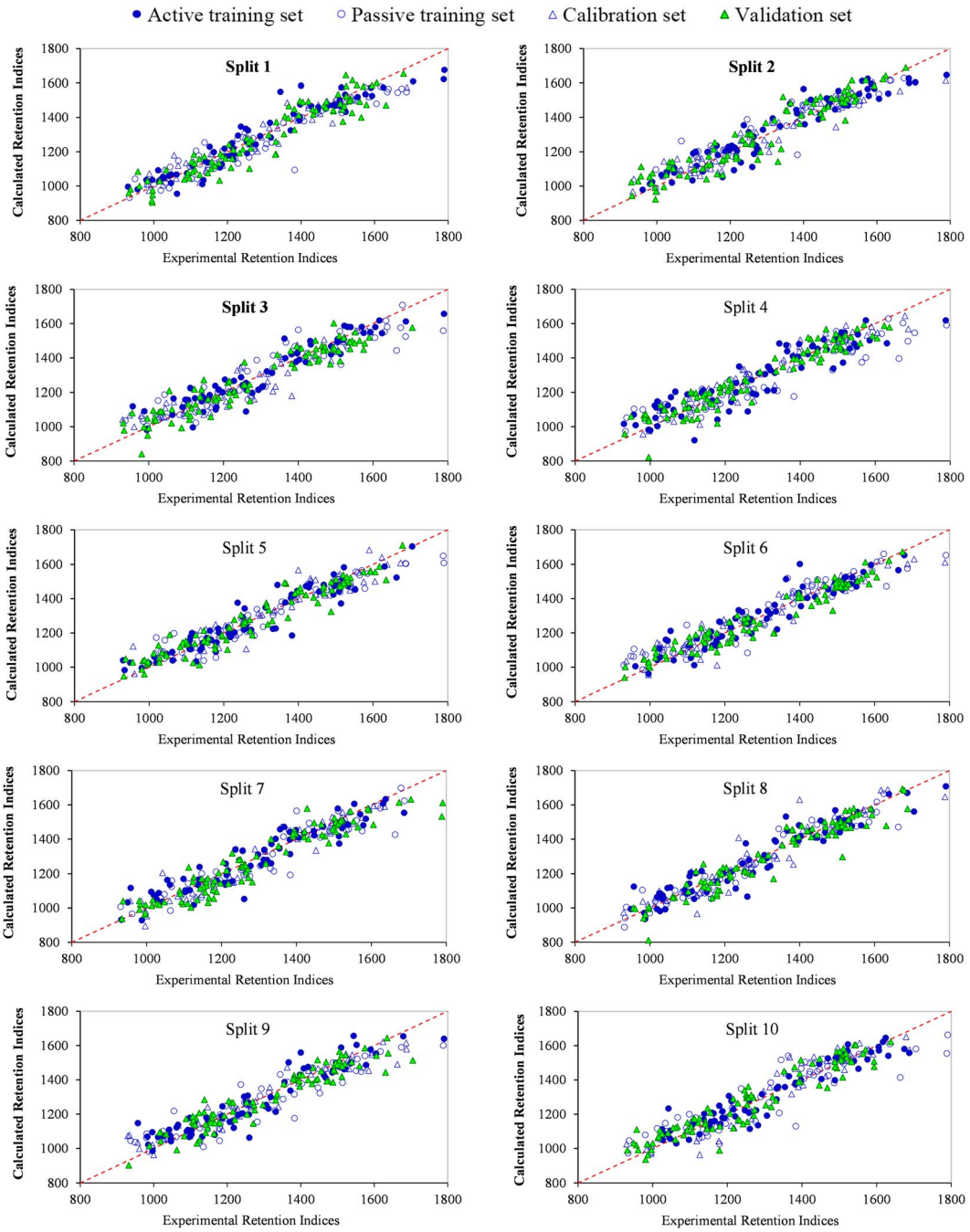

Fig. 2 Experimental *versus* predicted retention indices of split 1 to 10 for VOCs detected in peppers by the Monte Carlo method based on target function TF3.

correlation (IIC) and correlation intensity index (CII), are also addressed in this work, which were not studied in earlier work. In the present QSPR models, only one descriptor, DCW, was used to construct the QSPR models but in the previously reported model, four descriptors were applied. The numerical value of the determination coefficient (R_{val}^2) of the QSPR model generated with TF3 for split 6 is 0.9308, which is much better than the value for the reported model. Thus, the presented QSPR models are more robust and predictable.

3.5. External validation of the proposed models

An external dataset of 115 VOCs reported by Rojas *et al.*[32] was used to predict the RI of molecules outside the dataset for

Table 1 The list of the promoters RI increase and decrease from splits 6 calculated with TF3

No.	Structural attributes	CWs Probe 1	CWs Probe 2	CWs Probe 3	NSs	NSc	NSv	Defect [SAk]	Description
The promoters of RI increase									
1	EC0-H…1…	0.0509	0.16064	0.34295	68	58	54	0	Morgan extended connectivity of zero-order for hydrogen atom as 1
2	EC1-H…4…	0.18025	0.22099	0.18401	68	57	54	0	Morgan extended connectivity of first-order for hydrogen atom as 4
3	PT2-H…3…	0.16527	0.2584	0.3257	68	57	54	0	The number of paths of length 2 which started from a hydrogen atom is equal to 3
4	C⋯C……	0.44726	0.01345	0.30905	65	55	50	0.0003	The presence of two consecutive aliphatic carbons
5	EC1-C…7…	0.31326	0.46929	0.21017	63	56	50	0	Morgan extended connectivity of first-order for carbon atom as 7
6	VS2–H…6…	0.10836	0.05545	0.26739	63	56	50	0	6 as a sum of vertex degrees which take place at a topological distance of 2 relatively to hydrogen vertex
7	EC0-C…3…	0.56731	0.20537	0.33853	62	47	46	0.0006	Morgan extended connectivity of zero-order for carbon atom as 3
8	EC1-C…10	0.22378	0.25831	0.04221	61	52	47	0.0002	Morgan extended connectivity of first-order for carbon atom as 4
9	NNC-C…422	0.20503	0.01758	0.05181	60	53	48	0.0001	The nearest neighbours codes for carbon equal to 422
10	C…(…C…	0.29947	0.13954	0.33177	59	49	49	0.0004	Two sp3 hybridized carbon joined by branching
11	=……	0.15273	0.45098	0.39027	56	43	44	0.0001	Presence of double covalent bond
12	1……	0.26393	0.42999	0.64276	53	46	42	0	Presence of at least one ring
13	NNC-C…321	0.44352	0.72343	0.10398	53	39	38	0.0008	The nearest neighbours codes for carbon equal to 321
14	PT2-H…2…	0.06983	0.57052	0.40344	53	42	38	0.0008	The number of paths of length 2 which started from a hydrogen atom is equal to 2
15	PT2-C…5…	0.21029	0.22211	0.19676	52	42	39	0.0005	The number of paths of length 2 which started from a carbon atom is equal to 5
The promoters of RI decrease									
1	NNC-C…413	−0.08801	−0.07644	−0.57505	67	57	52	0.0002	The nearest neighbours codes for carbon equal to 413
2	C…1…(…	−0.30101	−0.02505	−0.28091	26	27	20	0.0003	Combination of aliphatic carbon, one ring and branching
3	NNC-C…440	−0.3105	−0.03567	−0.80092	26	27	20	0.0003	The nearest neighbours codes for carbon equal to 440
4	C⋯O…(…	−0.39833	−1.30355	−0.7525	8	1	4	0.0036	Combination of the carbon atom, oxygen and branching
5	O…(…(…	−0.15072	−1.42791	−2.29626	5	1	5	0.0019	Oxygen atom with two branching
6	VS2–C…28	−0.05713	−0.5657	−0.85747	5	8	4	0.0001	28 as a sum of vertex degrees which take place at a topological distance of 2 relatively to carbon vertex
7	3⋯C…1…	−1.16603	−0.21466	−2.69557	1	6	1	0.0019	

Table 2 Comparison of present QSPR models with the previously reported study

No.	Set	*n*	Descriptor generator	Regression method	R^2 train	RMSD	IIC	CII	Ref.
1	Training	92	Dragon and PaDEL	MLR	0.879	72.1	—	—	32
	Validation	91			0.832	91.7	—	—	
	Test	90			0.915	55.4	—	—	
2	ActivTRN	68	CORAL package	LR	0.885	62.7	0.658	0.928	Present work
	PassTRN	58			0.900	70.8	0.677	0.943	
	Calib	54			0.904	51.6	0.951	0.944	
	Valid	90			0.931	54.4	0.770	0.955	

modeling. The RI properties of these compounds were predicted by ten models based on TF3 and average values were compared with external predictions by Rojas *et al.* Table 3 shows the average predicted RI of ten models, the prediction by Rojas *et al.*[32] for the BPX5 and BP20 column coupled system, and experimental retention indices from the literature.

Fig. 3 shows a plot of the RI of the external set predicted by CORAL software *versus* the RI predicted by Rojas *et al.*.[32] There is good agreement between the external predictions by the two methods.

Table 3 External set of common VOCs detected in peppers: name, CAS registry number, predicted retention indices based on the average prediction of models 1 to 10, and prediction by Rojas *et al.*[32] for the BPX5 and BP20 column coupled system, experimental retention indices from the literature, and source

					Experimental $RI_{literature}$									
No.	Name	CAS number	$RI_{predicted}$ (this study)	$RI_{predicted}$ (Rojas *et al.*)	DB-5 column	HP-5MS stationary phase	HP-5 column	DB-Wax stationary phase	BPX5 column	RTX-Wax stationary phase	HP-20M column	DB-5MS stationary phase	BP20 column	Ref.
1	Myrcenol	543-39-5	1164.719	1159.6	NA	NA[a]	NA	NA	NA	NA	NA	NA	NA	41
2	(*E*,*E*)-α-Farnesene	502-61-4	1483.631	1496.2	1508	NA	NA	NA	NA	NA	NA	NA	NA	15, 42 and 43
	α-Farnesene		—	—		NA	NA	NA	NA	NA	NA	NA	NA	41 and 44
3	Elemicin	487-11-6	1501.785	1565	1540 1554 1556	NA	NA	NA	NA	NA	NA	NA	NA	43 and 45
4	Myristicin	607-91-0	1391.435	1546.5	1520	NA	NA	NA	NA	NA	NA	NA	NA	43
5	Apiole	523-80-8	1541.468	1721.7	1679 1680 1685	NA	NA	NA	NA	NA	NA	NA	NA	43
6	Dillapiole	484-31-1	1565.236	1709.1	1622 1644	1622	NA	NA	NA	NA	NA	NA	NA	14,43
7	Eugenol acetate	93-28-7	1568.772	1577.7	1524	NA	NA	NA	NA	NA	NA	NA	NA	45
8	Carvone oxide	18 383-49-8	1239.442	1367.3	NA	NA	NA	NA	NA	NA	NA	NA	NA	41, 42 and 46–49
	trans-Carvone oxide	33 204-74-9	—	—	NA	NA	NA	NA	NA	NA	NA	NA	NA	41
9	α-Bulnesene	3691-11-0	1484.066	1508.7	1493 1503 1505	1505	NA	NA	NA	NA	NA	NA	NA	41
	δ-Guaiene		—	—	NA	NA	NA	NA	NA	NA	NA	NA	NA	42 and 43
10	Dihydrocarveol	619-01-2	1164.505	1184.8	1192 1195	NA	1195	1941	NA	NA	NA	NA	NA	41, 42, 44 and 46–49
	p-Menth-8-en-2-ol		—	—	NA	NA	NA	NA	NA	NA	NA	NA	NA	42
	trans-*p*-Menth-8-en-2-ol		—	—	NA	NA	NA	NA	NA	NA	NA	NA	NA	47–49
	Neo-dihydrocarveol	18 675-34-8	—	—	NA	NA	NA	NA	NA	NA	NA	NA	NA	41
11	*cis*-β-Terpineol	138-87-4	1196.492	1181	1159	NA	NA	NA	NA	NA	NA	NA	NA	41
12	β-Bisabolol	15 352-77-9	1647.933	1604.1	NA	NA	1668	NA	NA	NA	2021	NA	NA	41 and 42
13	α-Bisabolol	515-69-5	1644.237	1594.9	1683 1701	NA	NA	NA	NA	NA	NA	NA	NA	14 and 44
14	Squalene	111-02-4	2742.641	2726	2790	NA	NA	NA	NA	NA	NA	NA	NA	6
15	δ-Terpinyl acetate	93 836-50-1	1382.135	1356	1313	NA	NA	NA	NA	NA	NA	NA	NA	41
16	1,4-Cineole	470-67-7	1139.433	1117.1	1016	1016	NA	1171	NA	NA	NA	NA	NA	41
17	Cadina,1,4-dien-3-ol		1608.026	1636.1	NA	NA	NA	NA	NA	NA	NA	NA	NA	41
18	*trans*-Piperitone oxide	4713-38-6	1194.878	1303.8	1258	NA	NA	NA	NA	NA	NA	NA	NA	50
19	3-Buten-2-ol	598-32-3	642.9435	758.6	NA	NA	NA	NA	NA	NA	NA	NA	NA	41

Table 3 (*Contd.*)

No.	Name	CAS number	$RI_{predicted}$ (this study)	$RI_{predicted}$ (Rojas *et al.*)	Experimental $RI_{literature}$									Ref.
					DB-5 column	HP-5MS stationary phase	HP-5 column	DB-Wax stationary phase	BPX5 column	RTX-Wax stationary phase	HP-20M column	DB-5MS stationary phase	BP20 column	
20	Vomifoliol	23 526-45-6	1573.99	1735.6	NA	1796	NA	3167 3175	1814	NA	NA	NA	NA	41
21	Neryl isovalerate	3915-83-1	1578.39	1593	NA	NA	NA	NA	NA	NA	NA	NA	1872	43
22	Retrofractamide B	54 794-74-0	2393.783	2624	NA	NA	NA	NA	NA	NA	NA	NA	NA	14
23	Guineensine	55 038-30-7	2568.907	2783.1	NA	NA	NA	NA	NA	NA	NA	NA	NA	14
24	Caryophyllene alcohol	472-97-9	1586.876	1548.9	1568	1560 1564	NA	NA	NA	NA	NA	NA	NA	42
	Caryophyllenol		—	—	NA	NA	NA	NA	NA	NA	NA	NA	NA	41, 44 and 46–49
25	Clovene	469-92-1	1440.777	1460	NA	NA	NA	NA	NA	NA	NA	NA	NA	42
26	Piperitol	491-04-3	1170.929	1143.6	NA	NA	NA	NA	NA	NA	NA	NA	NA	43
27	Humulene oxide II	19 888-34-7	1609.486	1589.6	1606 1607	NA	NA	NA	NA	NA	NA	NA	NA	41
28	α-Cedrene	469-61-4	1447.516	1451.9	1409 1410	1409	NA	NA	NA	1562	NA	NA	NA	43
29	Hedycaryol	21 657-90-9	1627.43	1612.5	1530	NA	NA	NA	NA	NA	NA	NA	NA	44
30	Germacrene D-4-ol	198 991-79-6	1594.602	1606.5	1511 1574	1567	NA	NA	NA	NA	NA	NA	NA	43
31	α-Eudesmol	473-16-5	1592.197	1595.8	1652	NA	NA	NA	NA	NA	2230	NA	NA	41 and 43
32	Furanodiene	19 912-61-9	1586.736	1626.1	NA	NA	NA	NA	NA	NA	NA	NA	NA	43
33	*cis-p*-Menth-8-en-2-ol		1180.423	1193.1	NA	NA	NA	NA	NA	NA	NA	NA	NA	47–49
34	Isopulegol	89-79-2	1200.764	1141.3	1145 1879	1146	NA	1879	NA	NA	NA	NA	NA	43
35	Menthol	89-78-1	1190.85	1113.6	1173 2103	NA	NA	1626	NA	NA	1646	NA	NA	41
36	*cis*-Sabinene hydrate	15 537-55-0	1144.655	975	1069 1070 1097	1101	NA	1465	NA	NA	NA	NA	NA	14 and 43
37	Cedrol	77-53-2	1583.856	1544.5	1596 1604	NA	NA	NA	NA	NA	NA	NA	NA	15, 41, 42 and 46–49
38	(*Z*)-Isosafrole	17 627-76-8	1271.586	1391.8	1308 1336	NA	NA	NA	NA	NA	NA	NA	NA	41
39	Nona-trans,*cis*-2,6-dienal	557-48-2	1102.993	1130.7	NA	NA	NA	1597 1605	NA	NA	NA	NA	NA	51
40	Howeveranediol	25 265-75-2	761.5132	733.4	NA	NA	NA	NA	NA	NA	NA	NA	NA	6
41	Ethyl-2-hexenol	50 639-00-4	993.1246	1003.4	NA	NA	NA	NA	NA	NA	NA	NA	NA	41
42	Hept-*trans*-3-en-2-one	1119-44-4	940.3034	900.1	NA	NA	NA	NA	NA	NA	NA	NA	NA	51

Table 3 (*Contd.*)

No.	Name	CAS number	$RI_{predicted}$ (this study)	$RI_{predicted}$ (Rojas *et al.*)	Experimental $RI_{literature}$									
					DB-5 column	HP-5MS stationary phase	HP-5 column	DB-Wax stationary phase	BPX5 column	RTX-Wax stationary phase	HP-20M column	DB-5MS stationary phase	BP20 column	Ref.
43	Nona-*trans*,*trans*-2,5- dien-4-one	61 759-51-1	1101.811	1085.6	NA	NA	NA	NA	NA	NA	NA	NA	NA	51
44	Hex-*trans*-2-enal	6728-26-3	838.5927	850.3	854	NA	857	1201	NA	NA	1209	848	NA	51
	(*E*)-2-Hexenal		—	—	NA	NA	NA	NA	NA	NA	NA	NA	NA	41
45	1-Hepten-3-ol	4938-52-7	902.912	925.4	NA	NA	NA	NA	NA	NA	NA	NA	NA	41
46	(*E*)-3-Octenol	18 185-81-4	1063.265	1043.7	NA	NA	NA	NA	NA	NA	NA	NA	NA	41
47	2-Heptanone	110-43-0	900.1747	971.3	888 889	NA	882	1160	889	NA	NA	NA	NA	51
48	Non-*trans*-2-en-4-one	32 064-72-5	1115.155	1156.7	NA	NA	NA	NA	NA	NA	NA	NA	NA	51
49	Non-1-en-4-one	61 168-10-3	1084.331	1154.4	NA	NA	NA	NA	NA	NA	NA	NA	NA	51
50	α-Ethyl hexanoate	123-66-0	1021.078	1118	996 997 998 1001	1001	997	1224 1229 1244 1270	NA	NA	NA	NA	NA	6
51	1-Octen-3-ol	3391-86-4	990.474	1013.3	942 978 980	975	977 991	980 1438 1465	NA	NA	1423	NA	NA	41
52	2,4-Decadienoic acid	42 997-42-2	1235.616	1736.5	NA	NA	NA	NA	NA	NA	NA	NA	NA	14
	Piperidide				NA	NA	NA	NA	NA	NA	NA	NA	NA	
53	Pellitorin	18 836-52-7	1519.16	1624.7	NA	NA	NA	NA	NA	NA	NA	NA	NA	14
54	Deca-*trans*,*cis*-2,4-dienal	25 152-83-4	1189.996	1212.5	1291 1297	NA	NA	1758	NA	NA	NA	NA	NA	51
	Deca-*trans*,*trans*-2,4-dienal	2363-88-4	—	—	NA	NA	NA	NA	NA	NA	NA	NA	NA	51
	Deca-2,4-dienal	25 152-84-5	—	—	1311 1314 1319	NA	NA	1820 1832	NA	NA	NA	NA	NA	51
55	(*E*)-2-Octenal	2363-89-5	1010.999	1023.6	NA	1060	NA	NA	NA	NA	NA	NA	NA	41
56	*N*-Isobutyl-(2*E*,4*E*,12*E*)-octadecatrienamide	943 546-17-6	2222.115	2290	NA	NA	NA	NA	NA	NA	NA	NA	NA	14
57	*N*-Isobutyl-(2*E*,4*E*,14*Z*)-eicosatrienamide	—	2397.239	2448.7	NA	NA	NA	NA	NA	NA	NA	NA	NA	14

Table 3 (*Contd.*)

No.	Name	CAS number	$RI_{predicted}$ (this study)	$RI_{predicted}$ (Rojas *et al.*)	Experimental $RI_{literature}$									
					DB-5 column	HP-5MS stationary phase	HP-5 column	DB-Wax stationary phase	BPX5 column	RTX-Wax stationary phase	HP-20M column	DB-5MS stationary phase	BP20 column	Ref.
58	Hexanal	66-25-1	836.3585	921.5	784 797 799 800 819	805	800 803	1067 1093	NA	NA	1075	NA	NA	16 and 51
59	2-Octanol	25 339-16-6	1019.923	981.9	NA	NA	NA	NA	NA	NA	NA	NA	NA	41
60	Nonane	111-84-2	964.4392	965.9	899	900	NA	NA	NA	NA	900	NA	NA	41
61	(*E*)-2-Tridecenal	7774-82-5	1448.809	1429.9	NA	NA	NA	NA	NA	NA	NA	NA	NA	43
62	Tetradecane	629-59-4	1402.249	1372.2	1116 1399	NA	NA	1399	1400	NA	1400	NA	NA	14
63	*N*-Isobutyl-(2*E*,4*E*)-octadecadienamide	54 794-70-6	2219.656	2266	NA	NA	NA	NA	NA	NA	NA	NA	NA	14
64	Pentadecanal	2765-11-9	1624.416	1660.3	1513 1687 1710	1711	NA	NA	NA	NA	NA	NA	NA	50
65	Hexadecane	544-76-3	1577.373	1531.4	1600	NA	NA	NA	NA	NA	1600	NA	NA	14
66	Palmitic acid	57-10-3	1755.653	1811.2	1984	NA	NA	NA	NA	NA	2860	NA	NA	14
	Palmitic acid glyceride		—	—	NA	NA	NA	NA	NA	NA	NA	NA	NA	6
67	Heptadecane	629-78-7	1664.935	1610.7	1700	NA	NA	NA	NA	NA	1700	NA	NA	14
68	1-Octadecene	112-88-9	1759.766	1711.6	1793 1794	NA	NA	NA	1774	NA	NA	NA	NA	14
69	Octadecane	593-45-3	1752.497	1689.9	1800	NA	NA	1805	NA	NA	1800	NA	NA	14
70	Nonadecane	629-92-5	1840.059	1768.9	1900	NA	NA	NA	NA	NA	1900	NA	NA	14
71	1-Eicosene	3452-07-1	1934.889	1869.5	1990 1994	NA	NA	NA	NA	NA	NA	NA	NA	14
72	Eicosane	112-95-8	1927.621	1847.8	2000	NA	NA	NA	NA	NA	2000	NA	NA	14
73	Heneicosane	629-94-7	2015.183	1926.7	2100	NA	NA	NA	NA	NA	2100	NA	NA	14
74	Docosane	629-97-0	2102.745	2005.4	2200	NA	NA	NA	NA	NA	2200	NA	NA	14
75	Nonadecanol	1454-84-8	2015.34	1901.6	NA	2156	NA	NA	NA	NA	NA	NA	NA	50
76	Hexanol	111-27-3	877.0338	846.4	867 884	NA	865	1351 1354 1360 1379 1392	NA	NA	1325	869	NA	41
77	Amyl alcohol	71-41-0	789.4719	751.3	766 768	NA	766	1244	NA	NA	NA	NA	NA	41
78	Benzenepropanoic acid, ethyl ester	2021-28-5	1339.896	1411.3	1390	NA	NA	1897 1905	NA	NA	NA	NA	NA	43

Table 3 (*Contd.*)

No.	Name	CAS number	$RI_{predicted}$ (this study)	$RI_{predicted}$ (Rojas *et al.*)	Experimental $RI_{literature}$									
					DB-5 column	HP-5MS stationary phase	HP-5 column	DB-Wax stationary phase	BPX5 column	RTX-Wax stationary phase	HP-20M column	DB-5MS stationary phase	BP20 column	Ref.
79	Methyl salicylate	119-36-8	1160.501	1248.3	1190 1191 1206	1190	NA	NA	NA	NA	NA	NA	NA	51
80	Guaiacol	90-05-1	1001.29	1087.9	1086 1091	NA	NA	1872 1875 1883	NA	NA	NA	NA	NA	41
81	2-Methoxy-3-isobutylpyrazine	24 683-00-9	1055.625	1291	1135 1171	NA	NA	1540	NA	NA	NA	NA	NA	51
82	Thymol	89-83-8	1189.021	1203.6	1290	1290	1308	NA	NA	NA	NA	NA	NA	41 and 43
83	2-Methylnaphthalene	91-57-6	1210.977	1379.3	1281	NA	1295	NA	NA	NA	NA	NA	NA	51
84	1-Methylnaphthalene	90-12-0	1163.889	1355.6	1298	NA	1312	NA	NA	NA	NA	NA	NA	51
85	Piperamide C 9:1 (8E)	62 510-52-5	2232.683	2552.6	NA	NA	NA	NA	NA	NA	NA	NA	NA	14
86	4,5-Dihydropiperettine	583-34-6	2105.33	2419.8	NA	NA	NA	NA	NA	NA	NA	NA	NA	14
87	Dehydropipernonaline	107 584-38-3	2279.967	2579.6	NA	NA	NA	NA	NA	NA	NA	NA	NA	14
88	Piperine	94-62-2	1928.943	2235.5	NA	NA	NA	NA	NA	NA	NA	NA	NA	14
89	Piperanine	23 512-46-1	1932.372	2211.5	NA	NA	NA	NA	NA	NA	NA	NA	NA	14
90	1-Cinnamoyl piperidine	5422-81-1	1597.08	1759.2	NA	NA	NA	NA	NA	NA	NA	NA	NA	14
91	Piperolein B	30 505-89-6	2301.005	2626.8	NA	NA	NA	NA	NA	NA	NA	NA	NA	14
92	Geranial	5392-40-5	1182.447	1151.7	1240	NA	NA	NA	NA	NA	NA	NA	NA	41
	Neral	106-26-3	—	—	1235 1240 1294	NA	NA	1630 1690 1695	NA	NA	1658	NA	NA	41
93	Citronella	106-23-0	1155.695	1216.9	1153 1159 1161	NA	NA	1425 1485 1488	NA	NA	NA	NA	NA	41, 42 and 46–49
94	Phenylacetaldehyde	122-78-1	1046.275	1112.2	1043 1049	NA	NA	1609 1671	NA	NA	1615	NA	NA	51
95	Furfural	98-01-1	753.1899	858.1	830	NA	NA	1458 1474 1485	832	NA	NA	NA	NA	51
96	Oxalic acid	144-62-7	740.7731	852.3	NA	NA	NA	NA	NA	NA	NA	NA	NA	6
97	α-Hydroxypropionic acid	50-21-5	699.8166	862.4	NA	NA	NA	NA	1058	NA	NA	NA	NA	6
98	Howeverenedioic acid	110-16-7	888.9371	943.8	NA	NA	NA	NA	NA	NA	NA	NA	NA	6
99	Dihydrolimonen-10-al	3269-90-7	1223.518	1236	NA	NA	NA	NA	NA	NA	NA	NA	NA	41
100	Gluconate anion	608-59-3	1350.775	1570.7	NA	NA	NA	NA	NA	NA	NA	NA	NA	6

Table 3 (*Contd.*)

No.	Name	CAS number	$RI_{predicted}$ (this study)	$RI_{predicted}$ (Rojas *et al.*)	Experimental $RI_{literature}$ DB-5 column	HP-5MS stationary phase	HP-5 column	DB-Wax stationary phase	BPX5 column	RTX-Wax stationary phase	HP-20M column	DB-5MS stationary phase	BP20 column	Ref.
101	Erythritol	149-32-6	943.4734	1041.8	NA	NA	NA	NA	NA	NA	NA	NA	NA	6
102	Glycerin	56-81-5	758.5946	864.6	NA	NA	NA	NA	NA	NA	NA	NA	NA	6
103	Myrtenol	515-00-4	1159.949	1118.5	1194 1196 1202 1214	NA	NA	NA	NA	NA	NA	NA	NA	42, 44 and 47–49
104	*cis-p*-Menth-2-en-7-oI		1185.016	1202.4	NA	NA	NA	NA	NA	NA	NA	NA	NA	41
105	Glucopyranose	492-62-6	1317.003	1440.1	NA	NA	NA	NA	NA	NA	NA	NA	NA	6
106	Geraniol	106-24-1	1175.015	1171.8	1255 1276	NA	1240	1788 1850 1862	NA	NA	1814	NA	NA	41
	Nerol	106-25-2	–	–	1228	NA	NA	1753	NA	NA	1770	NA	NA	41 and 50
107	(2*E*,6*E*)-Farnesol	106-28-5	1606.869	1597.8	1706 1722	NA	NA	2371	NA	NA	NA	NA	NA	43
	(*E*,*E*)-Farnesol		–	–	NA	NA	NA	NA	NA	NA	NA	NA	NA	41
	α-Farnesol		–	–	NA	NA	NA	NA	NA	NA	NA	NA	NA	44
	(*Z*,*Z*)-Farnesol	4602-84-0	–	–	1689 1713 1718	1713	1713	NA	NA	NA	NA	NA	NA	41
	(2*Z*,6*Z*)-Farnesol		–	–	NA	NA	NA	NA	NA	NA	NA	NA	NA	43
	(2*E*,6*Z*)-Farnesol	3879-60-5	–	–	1734 1742 1748	1742 1743	NA	NA	NA	NA	NA	NA	NA	43
	(*E*,*Z*)-Farnesol		–	–	NA	NA	NA	NA	NA	NA	NA	NA	NA	41
	(*Z*,*E*)-Farnesol	3790-71-4	–	–	1697	NA	NA	NA	NA	NA	NA	NA	NA	41
108	Phytol	150-86-7	1941.848	1928.7	1949	NA	NA	NA	NA	NA	2571	NA	NA	43
109	(*E*)-Cinnamyl alcohol	4407-36-7	1155.272	1238.7	1305	NA	NA	NA	NA	NA	NA	NA	NA	41
110	2-Methyl cinnamyl alcohol	1504-55-8	1212.211	1285.1	NA	NA	NA	NA	NA	NA	NA	NA	NA	41
111	Isoamyl alcohol	123-51-3	764.7509	679.6	734 735	NA	737	1169 1206 1230	NA	NA	1182	NA	NA	41
112	Hex-*cis*-3-enol	928-96-1	880.2674	870.4	857	NA	NA	1378 1401 1407	NA	NA	1357	849	NA	51
	3-Hexenol	544-12-7	–	–	NA	NA	NA	NA	NA	NA	NA	NA	NA	41
113	Cumin alcohol	536-60-7	1204.248	1262.4	1287	NA	NA	2099	NA	NA	NA	NA	NA	41
114	Biphenyl	92-52-4	1283.923	1486.7	1381	NA	1385	NA	NA	NA	NA	NA	NA	51
115	Naphthalene	91-20-3	1131.721	1316	1179	NA	NA	NA	NA	NA	1718	NA	NA	51

[a] Not available.

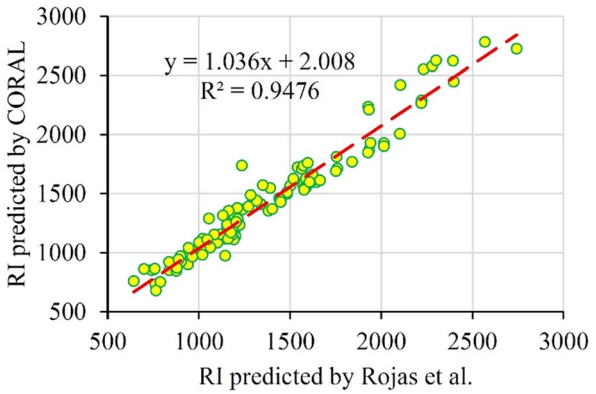

Fig. 3 Plot of the RI of external set predicted by CORAL software *versus* the RI predicted by Rojas *et al.*

4. Conclusions

In the present study, 40 QSPR models for the prediction of RI of 273 VOCs were developed from 10 random splits. The balance of correlation algorithm was used to design QSRR models. Four target functions, *i.e.* TF_0 (without IIC or CII), TF_1 (with IIC alone), TF_2 (with CII alone) and TF_3 (with IIC and CII, simultaneously) were employed to verify the significance of the present statistical method of QSPR model generation. The simultaneous use of IIC and CII (TF_3) improves the predictive potential of the QSPR model. All suggested models render satisfactory predictive QSPR models for the RI of the VOCs, but the best predictive potential was computed withTF_3 for split 6; thus it is specified as the best model. To evaluate the reliability and prediction ability of all created models, various statistical parameters, such as R^2, IIC, CII, CCC, Q^2, $Q_{F1}2$, $Q_{F2}2$, $Q_{F3}2$, s, MAE, F, RMSE, $\overline{R_m^2}$, $\overline{\Delta R_m^2}$, CR_p^2 and Y-test were utilized. A comparison of some statistical parameters of the present study, as analyzed by the QSPR model developed by Rojas *et al.*[32] reveals that the R^2 value for the training set has shown an improvement, increasing from 0.879 to 0.900. Similarly, the R^2 value for the test set has also demonstrated an enhancement, rising from 0.915 to 0.931. In addition, the RMSD has exhibited a reduction, decreasing from 72.1 to 62.7 for the training set and from 55.4 to 54.4 for the test set. The applicability domain (AD) was studied based on "statistical defect" d(A). The structural attributes based on graph invariants and SMILES notation were also extracted from the split 6 (best model) and employed to recognize the promoters of RI increase and decrease. Morgan extended connectivity of zero-order for hydrogen atom as 1 (ec0-h…1…), Morgan extended connectivity of first-order for hydrogen atom as 4 (ec1-h…4…), Morgan extended connectivity of first-order for carbon atom as 7 (ec1-c…7…), Morgan extended connectivity of zero-order for carbon atom as 3 (ec0-c…3…), Morgan extended connectivity of first-order for carbon atom as 4 (ec1-c…10…) *etc* were some significant promoters of endpoint increase. The nearest neighbours codes for carbon equal to 413 (nnc-c…413), the nearest neighbours codes for carbon equal to 440 (nnc-c…440), a combination of the carbon atom, oxygen and branching (c…o…(…), and 28 as a sum of vertex degrees which take place at a topological distance of 2 relatively to carbon vertex (*vs.* 2-c…28) *etc* are some significant promoters of endpoint decrease.

Data availability

The datasets used and/or analysed during the current study are available from the corresponding author on reasonable request.

Conflicts of interest

There are no conflicts to declare.

References

1 R. Sharma, V. K. Joshi and M. Kaushal, Effect of pre-treatments and drying methods on quality attributes of sweet bell-pepper (Capsicum annum) powder, *J. Food Sci. Technol.*, 2015, **52**(6), 3433–3439.
2 G. Guclu, D. Keser, H. Kelebek, M. Keskin, Y. E. Sekerli, Y. Thereforeysal and S. Selli, Impact of production and drying methods on the volatile and phenolic characteristics of fresh and powdered sweet red peppers, *Food Chem.*, 2021, **338**, 128129.
3 L. Gorgani, M. Mohammadi, G. D. Najafpour and M. Nikzad, Piperine—the bioactive compound of black pepper: from isolation to medicinal formulations, *Compr. Rev. Food Sci. Food Saf.*, 2017, **16**(1), 124–140.
4 A. Musenga, R. Mandrioli, A. Ferranti, G. D'Orazio, S. Fanali and M. A. Raggi, Analysis of aromatic and terpenic constituents of pepper extracts by capillary electrochromatography, *J. Separ. Sci.*, 2007, **30**(4), 612–619.
5 C. Taiti, C. Costa, C. A. Migliori, D. Comparini, S. Figorilli and S. Mancuso, Correlation between volatile compounds and spiciness in domesticated and wild fresh chili peppers, *Food Bioprocess Technol.*, 2019, **12**(8), 1366–1380.
6 Q. Huo, Z. Wang, S. Xiong and R. Shi, Determination of volatile organic compounds in pepper seeds by GC/MS, *Asian J. Chem.*, 2013, **25**(16), 8909–8912.
7 S. K. Malhotra and K. Peter, *Handbook of Herbs and Spices*, Woodhead Publishing Series in Food Science, Technology and Nutrition, 2012, vol. 2.
8 G. Singh, P. Marimuthu, C. Catalan and M. DeLampasona, Chemical, antioxidant and antifungal activities of volatile oil of black pepper and its acetone extract, *J. Sci. Food Agric.*, 2004, **84**(14), 1878–1884.
9 K. L. Driffield, L. Mooney and K. G. Kerr, Temperature-dependent Changes in Susceptibility of Stenotrophomonas maltophilia. To the Essential Oils of Sweet Basil (Ocimum basilicum.) and Black Pepper (Piper nigrum.), *Pharmaceut. Biol.*, 2006, **44**(2), 113–115.
10 C. Taiti, C. Costa, P. Menesatti, D. Comparini, N. Bazihizina, E. Azzarello, E. Masi and S. Mancuso, Class-modeling approach to PTR-TOFMS data: a peppers case study, *J. Sci. Food Agric.*, 2015, **95**(8), 1757–1763.

11 M. Plessi, D. Bertelli and F. Miglietta, Effect of microwaves on volatile compounds in white and black pepper, *LWT–Food Sci. Technol.*, 2002, **35**(3), 260–264.
12 Y. Murakami, H. Iwabuchi, Y. Ohba and H. Fukami, Analysis of volatile compounds from chili peppers and characterization of Habanero (Capsicum chinense) volatiles, *J. Oleo Sci.*, 2019, **68**(12), 1251–1260.
13 Y. Murakami, H. Iwabuchi, M. Horikawa, S. Mori, Y. Ohba and H. Fukami, Isolation and Identification of a Volatile Compound in Habanero Pepper (Capsicum chinense), *J. Oleo Sci.*, 2018, **67**(10), 1219–1225.
14 I. Kapoor, B. Singh, G. Singh, C. S. De Heluani, M. De Lampasona and C. A. Catalan, Chemistry and in vitro antioxidant activity of volatile oil and oleoresins of black pepper (Piper nigrum), *J. Agric. Food Chem.*, 2009, **57**(12), 5358–5364.
15 B. Mamatha, M. Prakash, S. Nagarajan and K. Bhat, Evaluation of the flavor quality of pepper (Piper nigrum L.) cultivars by GC-MS, electronic nose and sensory analysis techniques, *J. Sensory Stud.*, 2008, **23**(4), 498–513.
16 Z. d. L. Cardeal, M. Gomes da Silva and P. Marriott, Comprehensive two-dimensional gas chromatography/mass spectrometric analysis of pepper volatiles, *Rapid Commun. Mass Spectrom.*, 2006, **20**(19), 2823–2836.
17 S. Ahmadi, A. Abdolmaleki and M. Jebeli Javan, in *Silico Study of Natural Antioxidants, Vitamins and Hormones*, Academic Press, 2022.
18 A. Kumar and P. Kumar, Cytotoxicity of quantum dots: use of quasiSMILES in development of reliable models with index of ideality of correlation and the consensus modelling, *J. Hazard. Mater.*, 2021, **402**, 123777.
19 P. Kumar, A. Kumar, S. Lal, D. Singh, S. Lotfi and S. Ahmadi, CORAL: Quantitative Structure Retention Relationship (QSRR) of flavors and fragrances compounds studied on the stationary phase methyl silicone OV-101 column in gas chromatography using correlation intensity index and consensus modelling, *J. Mol. Struct.*, 2022, **1265**, 133437.
20 S. Lotfi, S. Ahmadi and P. Kumar, The Monte Carlo approach to model and predict the melting point of imidazolium ionic liquids using hybrid optimal descriptors, *RSC Adv.*, 2021, **11**(54), 33849–33857.
21 A. Toropov, A. Toropova, G. Selvestrel and E. Benfenati, Idealization of correlations between optimal simplified molecular input-line entry system-based descriptors and skin sensitization, *SAR QSAR Environ. Res.*, 2019, **30**(6), 447–455.
22 A. P. Toropova, A. A. Toropov, R. Rallo, D. Leszczynska and J. Leszczynski, Optimal descriptor as a translator of eclectic data into prediction of cytotoxicity for metal oxide nanoparticles under different conditions, *Ecotoxicol. Environ. Saf.*, 2015, **112**, 39–45.
23 A. A. Toropov and A. P. Toropova, The Correlation Contradictions Index (CCI): building up reliable models of mutagenic potential of silver nanoparticles under different conditions using quasi-SMILES, *Sci. Total Environ.*, 2019, **681**, 102–109.
24 P. Kumar and A. Kumar, CORAL: QSAR models of CB1 cannabinoid receptor inhibitors based on local and global SMILES attributes with the index of ideality of correlation and the correlation contradiction index, *Chemom. Intell. Lab. Syst.*, 2020, **200**, 103982.
25 A. P. Toropova, A. A. Toropov, E. Carnesecchi, E. Benfenati and J. L. Dorne, The using of the Index of Ideality of Correlation (IIC) to improve predictive potential of models of water solubility for pesticides, *Environ. Sci. Pollut. Res.*, 2020, **27**(12), 13339–13347.
26 A. A. Toropov, R. Carbó-Dorca and A. P. Toropova, Index of Ideality of Correlation: new possibilities to validate QSAR: a case study, *Struct. Chem.*, 2018, **29**(1), 33–38.
27 S. Lotfi, S. Ahmadi and P. Kumar, A hybrid descriptor based QSPR model to predict the thermal decomposition temperature of imidazolium ionic liquids using Monte Carlo approach, *J. Mol. Liq.*, 2021, **338**, 116465.
28 P. Achary, A. Toropova and A. Toropov, Combinations of graph invariants and attributes of simplified molecular input-line entry system (SMILES) to build up models for sweetness, *Food Res. Int.*, 2019, **122**, 40–46.
29 T. Ghiasi, S. Ahmadi, E. Ahmadi, M. Talei Bavil Olyai and Z. Khodadadi, The index of ideality of correlation: QSAR studies of hepatitis C virus NS3/4A protease inhibitors using SMILES descriptors, *SAR QSAR Environ. Res.*, 2021, **32**(6), 495–520.
30 S. Ahmadi, A. P. Toropova and A. A. Toropov, Correlation intensity index: mathematical modeling of cytotoxicity of metal oxide nanoparticles, *Nanotoxicology*, 2020, **14**(8), 1118–1126.
31 A. A. Toropov and A. P. Toropova, Correlation intensity index: building up models for mutagenicity of silver nanoparticles, *Sci. Total Environ.*, 2020, **737**, 139720.
32 C. Rojas, P. R. Duchowicz and E. A. Castro, Foodinformatics: Quantitative Structure-Property Relationship Modeling of Volatile Organic Compounds in Peppers, *J. Food Sci.*, 2019, **84**(4), 770–781.
33 R. Singh, P. Kumar, M. Devi, S. Lal, A. Kumar, J. Sindhu, A. P. Toropova, A. A. Toropov and D. Singh, Monte Carlo based QSGFEAR: prediction of Gibb's free energy of activation at different temperatures using SMILES based descriptors, *New J. Chem.*, 2022, **46**(39), 19062–19072.
34 P. Kumar, A. Kumar and D. Singh, CORAL: development of a hybrid descriptor based QSTR model to predict the toxicity of dioxins and dioxin-like compounds with correlation intensity index and consensus modelling, *Environ. Toxicol. Pharmacol.*, 2022, **93**, 103893.
35 A. Kumar, P. Kumar and D. Singh, QSRR modelling for the investigation of gas chromatography retention indices of flavour and fragrance compounds on Carbowax 20 M glass capillary column with the index of ideality of correlation and the consensus modelling, *Chemometr. Intelligent Lab. Syst.*, 2022, **224**, 104552.
36 M. Duhan, J. Sindhu, P. Kumar, M. Devi, R. Singh, R. Kumar, S. Lal, A. Kumar, S. Kumar and K. Hussain, Quantitative structure activity relationship studies of novel hydrazone

derivatives as α-amylase inhibitors with index of ideality of correlation, *J. Biomol. Struct. Dyn.*, 2022, **40**(11), 4933–4953.
37 A. P. Toropova, A. A. Toropov, J. B. Veselinović, F. N. Miljković and A. M. Veselinović, QSAR models for HEPT derivates as NNRTI inhibitors based on Monte Carlo method, *Eur. J. Med. Chem.*, 2014, **77**, 298–305.
38 S. Ahmadi and A. Akbari, Prediction of the adsorption coefficients of some aromatic compounds on multi-wall carbon nanotubes by the Monte Carlo method, *SAR QSAR Environ. Res.*, 2018, **29**(11), 895–909.
39 A. A. Toropov and A. P. Toropova, QSAR as a random event: criteria of predictive potential for a chance model, *Struct. Chem.*, 2019, **30**(5), 1677–1683.
40 S. Ahmadi, Z. Moradi, A. Kumar and A. Almasirad, SMILES-based QSAR and molecular docking study of xanthone derivatives as α-glucosidase inhibitors, *J. Recept. Signal Transduction*, 2022, **42**(4), 361–372.
41 A. N. Menon, S. Chacko and C. Narayanan, Free and glycosidically bound volatiles of pepper (Piper nigrum L.), *J. Essent. Oil Res.*, 2001, **13**(3), 166–169.
42 M. Gopalakrishnan, N. Menon, K. Padmakumari, A. Jayalekshmy and C. Narayanan, GC Analysis and Odor Profiles of Four New Indian Genotypes of Piper nigrum L, *J. Essent. Oil Res.*, 1993, **5**(3), 247–253.
43 A. Martins, L. Salgueiro, R. Vila, F. Tomi, S. Canigueral, J. Casanova, A. P. Da Cunha and T. Adzet, Essential oils from four Piper species, *Phytochemistry*, 1998, **49**(7), 2019–2023.
44 A. Orav, I. Stulova, T. Kailas and M. Müürisepp, Effect of storage on the essential oil composition of Piper nigrum L. fruits of different ripening states, *J. Agric. Food Chem.*, 2004, **52**(9), 2582–2586.
45 J. K. R. Da Silva, J. R. A. Silva, S. B. Nascimento, S. F. Da Luz, E. N. Meireles, C. N. Alves, A. R. Ramos and J. G. S. Maia, Antifungal activity and computational study of constituents from Piper divaricatum essential oil against Fusarium infection in black pepper, *Molecules*, 2014, **19**(11), 17926–17942.
46 A. N. Menon and K. Padmakumari, Essential oil composition of four major cultivars of black pepper (Piper nigrum L.)—IV, *J. Essent. Oil Res.*, 2005, **17**(2), 206–208.
47 A. N. Menon and K. Padmakumari, Studies on essential oil composition of cultivars of black pepper (Piper nigrum L.)—V, *J. Essent. Oil Res.*, 2005, **17**(2), 153–155.
48 A. N. Menon, K. Padmakumari and A. Jayalekshmy, Essential oil composition of four major cultivars of black pepper (Piper nigrum L.) III, *J. Essent. Oil Res.*, 2003, **15**(3), 155–157.
49 A. N. Menon, K. Padmakumari, A. Jayalekshmy, M. Gopalakrishnan and C. Narayanan, Essential oil composition of four popular Indian cultivars of black pepper (Piper nigrum L.), *J. Essent. Oil Res.*, 2000, **12**(4), 431–434.
50 D. Sruthi, J. T. Zachariah, N. Leela and K. Jayarajan, Correlation between chemical profiles of black pepper (Piper nigrum L.) var. Panniyur-1 collected from different locations, *J. Med. Plants Res.*, 2013, **7**(31), 2349–2357.
51 R. Howevertery, R. Seifert, D. Guadagni and L. Ling, Characterization of some volatile constituents of bell peppers, *J. Agric. Food Chem.*, 1969, **17**(6), 1322–1327.